

# Three-dimensional steady disturbance modes in the Blasius boundary layer – a DNS study

Markus Kloker and Christian Stemmer

Institut für Aerodynamik und Gasdynamik, Universität Stuttgart,  
Pfaffenwaldring 21, D-70550 Stuttgart, Germany  
(last name)@iag.uni-stuttgart.de,  
www.iag.uni-stuttgart.de

## Summary

Direct numerical simulation is used to investigate the nature and behaviour of steady spanwise flow modulations excited internally in the Blasius boundary layer, primarily for a Reynolds number based on the displacement thickness ( $Re_{\delta_1}$ ) greater than 1,600. Both types of disturbances known –  $u'$ -streak-/Klebanoff modes or longitudinal vortex modes – exhibit a periodic spanwise variation, but the  $u'$ -modes are characterized by a dominant streamwise disturbance velocity component and a negligible swirling motion, whereas for the vortex modes the latter is strong. We investigate how the respective modes can be identified and in which situation they are present, using direct excitation at the wall locally as well as non-locally, and nonlinear generation in the oblique and fundamental breakdown scenario in transition to turbulence. Understanding their occurrence contributes to understanding non-eigenmodal disturbance growth and secondary flow instability eventually causing final laminar breakdown.

## 1 Introduction

During the past decade an intensification of research on receptivity and algebraic growth of boundary-layer disturbances has taken place to elucidate laminar-turbulent transition scenarios occurring at streamwise stations where no or only a weak classical Tollmien-Schlichting (TS) instability exists. This is the case for subcritical  $Re_{\delta_1}$ , or for larger  $Re_{\delta_1}$  where only very low-frequency TS-modes are weakly amplified if no adverse pressure gradient is present. Such scenarios are called bypass transition. On the one hand non-exponential growth of unsteady initial disturbances is considered, mostly dealing with an optimized superposition of (unstable) Orr-Sommerfeld and stable Squire eigenmodes to minimize the initial streamwise velocity disturbance  $u'$  and hence the energy (see, e.g., [6, 4, 5]). Note that Orr-Sommerfeld modes possess a wall-normal ( $y$ -) velocity disturbance  $v'$  whereas Squire modes do not, and a superposition can yield an almost arbitrary  $u'(y)$  profile with the  $v'(y)$ -profile of the Orr-Sommerfeld mode. Once existing, such a disturbance transiently grows in  $u'$  – by decay of its Squire components – to reach the eigenmode state. On the

other hand the growth of steady disturbances is investigated for which no amplified eigenmodes exist in the Blasius flow. These disturbances consist of modes of the continuous part of the eigenmode spectrum and typically lead to high- and low-velocity streaks in the boundary layer. Because they are not simply amenable to analysis by the standard Orr-Sommerfeld theory, often an adapted parabolic linear theory is used (see, e.g., [7, 2, 3, 1, 9]). It is sometimes claimed that any steady spanwise boundary-layer modulation grows unavoidably in a transient fashion due to the streamwise-momentum “lift-up” effect induced by a positive wall-normal disturbance velocity  $v'$ . Such an effect must strongly depend on the ratio of  $|v'|/|u'|$ .

Relevant nonlinear generation/involvement of a 3-d steady flow modulation occurs either in K-breakdown, induced by a large 2-d TS wave and a symmetrical pair of smaller oblique waves of the same frequency, or in the oblique-type breakdown, induced exclusively by the oblique wave pair. In the airfoil boundary layer considered in the main course of the DFG project underlying this work breakdown scenarios initiated by a point-source disturbance at the wall have been investigated and found to be dominated by a multitude of oblique waves [10, 11]. To clarify the basic nature and role of the steady spanwise flow modulations we compare steady modes excited directly at the wall with modes generated nonlinearly in the boundary layer, like in the oblique-breakdown and fundamental-breakdown scenario. Moreover, we wanted to check the feasibility of such investigations by direct numerical simulations in order to complement findings by theory.

## 2 Numerical Method

The extensively verified and validated numerical method is based on the complete Navier-Stokes equations for incompressible, 3-d unsteady flow in the vorticity-velocity formulation and the spatial model. The equations are solved in a disturbance formulation. For this purpose, the system is split in a 2-d steady base flow, here Blasius-type flow as a Navier-Stokes solution, and the 3-d disturbance flow, denoted by a prime. The utilized variables are nondimensionalized with the reference velocity  $\tilde{U}_\infty = 54.4 \text{ m s}^{-1}$ , and the length  $\tilde{L} = 0.0465 \text{ m}$ ; the kinematic viscosity is  $\tilde{\nu} = 1.71 \times 10^{-5} \text{ m}^2 \text{ s}^{-1}$ . The global reference Reynolds number is  $Re = 147930$ . Variables with a tilde denote dimensional variables. The vorticities are defined as

$$\omega_x = \frac{\partial v}{\partial z} - \frac{\partial w}{\partial y}, \quad \omega_y = \frac{\partial w}{\partial x} - \frac{\partial u}{\partial z}, \quad \omega_z = \frac{\partial u}{\partial y} - \frac{\partial v}{\partial x}. \quad (1)$$

For the integration domain and the coordinate system see fig. 1.

The numerical scheme employs fourth-order accurate finite differences in streamwise and wall-normal direction, and a fourth-order accurate Runge-Kutta time stepping. The spanwise direction is discretized through Fourier modes exploiting periodic boundary conditions in this direction. At the inflow boundary, all disturbances are set to zero; at the wall the no-slip and impermeability conditions apply except for the disturbance strip where a defined wall-normal velocity  $v'$  is prescribed. At the outflow boundary, a well-tested damping-zone technique is applied. At the upper

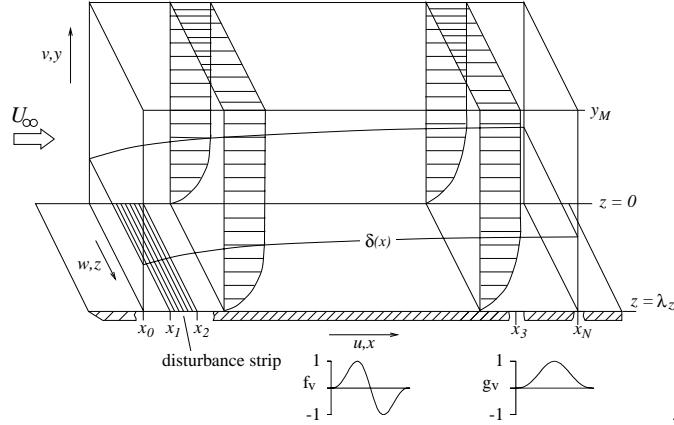


**Figure 1** Integration domain and disturbance functions.

boundary, the disturbance vorticities vanish and for the wall-normal velocity exponential decay is enforced. The details of the applied numerical method are described in [10, 8]. The examined modes are presented in the frequency–spanwise wave number spectrum  $(h, k)$ , where  $h$  denotes the multiples of the basic disturbance frequency ( $\beta = 2\pi\tilde{L}\tilde{f}/\tilde{U}_\infty = 9.45$ ;  $F = 2\pi\tilde{f}\tilde{\nu}/\tilde{U}_\infty^2 = 63.8$ ) and  $k$  marks multiples of the basic spanwise wave number ( $\gamma = 6.6$ ). Due to the imposed flow-field symmetry with respect to  $z=0$ , the modes  $(h > 0, \pm k)$  are identical in amplitude and typically referred to as the mode  $(h > 0, k)$  that has the double amplitude value. Furthermore,  $\omega_x = \omega'_x$ ,  $\omega_y = \omega'_y$  and  $w = w'$  due to the symmetry and the 2-d base flow.

In the simulations, disturbances are introduced at the wall through a localized disturbance strip within  $x_1=6.0$  and  $x_2=6.25$  (except for cases 2 and 4),  $x_2 - x_1 \approx 8\delta$ ,  $\delta$  – boundary-layer thickness, and

$$v'(x, 0, z, t) = (A_g(k) \cdot g_v(x) + A_f(h, k) \cdot f_v(x) \sin(h\beta t + \varphi(h, k))) \cdot \cos k\gamma z; \quad (2)$$

$g_v(x)$  and  $f_v(x)$  are 5<sup>th</sup> order parabolas, see fig. 1; at their ends the first and second x-derivatives are zero. The parameters of the various cases are compiled in table 1.

The resolution in the presented cases was  $\Delta x = \Delta\tilde{x}/\tilde{L} = 0.00655$ ,  $\Delta y = \Delta\tilde{y}/\tilde{L} = 0.000482$ ,  $\Delta z = \Delta\tilde{z}/\tilde{L} = 0.079$  and  $\Delta t = \Delta\tilde{t}\tilde{U}_\infty/\tilde{L} = 0.00665$ . The height of the integration domain comprised about 3.5 boundary layer thicknesses  $\delta$  at the inflow boundary and about 2.2  $\delta$  at the outflow boundary  $x_E = 13.2$  for, e.g., case 1. The number of points in the wall-normal direction was 225. We note that for the time transients to die out, a large number of time steps is necessary to achieve converged results for the  $(0, k)$  components, both in steady and unsteady cases.

**Table 1** Disturbance parameters for the various cases.

case	mode	$A_f$	$A_g$	$Re_{\delta_1}(x_1) - Re_{\delta_1}(x_2)$	$\varphi$
1	(1,0)	$3.6 \times 10^{-4}$	0.0	1,621 - 1,655	0
	(1,1)	$3.6 \times 10^{-4}$	0.0	1,621 - 1,655	0
2	(1,1)	$3.6 \times 10^{-4}$	0.0	683 - 762	0
3	(0,2)	0.0	$3.6 \times 10^{-5}$	1,621 - 1,655	0
4	(0,2)	0.0	$3.6 \times 10^{-5}$	1,621 - 2,331	0
5	(1,0)	$4.0 \times 10^{-3}$	0.0	1,621 - 1,655	0
	(0,1)	0.0	$3.6 \times 10^{-4}$	1,621 - 1,655	0
6	(1,0)	$4.0 \times 10^{-3}$	0.0	1,621 - 1,655	0
	(1,1)	$7.2 \times 10^{-4}$	0.0	1,621 - 1,655	0
7	(1,0)	$4.0 \times 10^{-3}$	0.0	1,621 - 1,655	0
	(1,1)	$7.2 \times 10^{-4}$	0.0	1,621 - 1,655	$\pi/2$

### 3 Results

#### 3.1 Steady modes generated locally upon nonlinearity

The streamwise location of the strip in the Blasius boundary layer was close to branch II of the instability curve for the chosen frequency  $\beta=9.45$ ,  $\tilde{f}=1760$  Hz. In case 1, the excited oblique waves  $(1, \pm 1)$  with an obliqueness angle of about  $\pm 15^\circ$  generate nonlinearly a  $(0,2)$  mode, and together with the excited  $(1,0)$  a  $(0,1)$  mode. Recall that upon nonlinearity, the modes  $(h_1, \pm k_1)$  and  $(h_2, \pm k_2)$  generate modes  $(h_1 \pm h_2, k_1 \pm k_2)$ , where the signs for  $h$  and  $k$  are not coupled and where also  $h_1 = h_2, k_1 = k_2$  is valid. The unsteady waves are small and experience attenuation in the further downstream development, thus a local nonlinear and independent generation of  $(0,1)$  and  $(0,2)$  near the location of the introduced disturbances is present. Modes  $(0,1)$  and  $(0,2)$  have an amplitude (maximum over  $y$ ) of  $u'/U_\infty = 10^{-5.5} \approx (10^{-2.7})^2$ , and  $|u'(0,1)|$  and  $|u'(0,2)|$  grow transiently along  $x$ , but eventually keep almost constant despite the decay of the generating modes. Moreover,  $v'$  and  $w'$  are decaying at the same time leading to modes with dominant  $u'$ : ( $|u'(0,1)| \approx 1000 \cdot |v'| \approx 50 \cdot |w'|$ ), ( $|u'(0,2)| \approx 300 \cdot |v'| \approx 80 \cdot |w'|$ ). Thus  $(0,1)$  and  $(0,2)$  are autonomous once generated and are not distinct eigenmodes. This was also verified through the simulation where the mode  $(1,1)$  was filtered out after the mode  $(0,2)$  was generated. The modes  $(0,1)$  and  $(0,2)$  were unaltered compared to the non-filtered case. Clearly, the modes  $(1,k)$  are only necessary here to generate the modes  $(0,k)$  nonlinearly. The further downstream development of the  $(0,k)$  modes is totally unaffected by the presence of the unsteady modes as long as their amplitudes remain at a level where the nonlinear generation of modes  $(0,k)$  through mode  $(1,k)$  is smaller than the actual amplitude of the mode  $(0,k)$ .

Before discussing the amplitudes of other disturbance components with figure 3, positioned for easy comparison with figure 2, we proceed with flow-field visualizations.

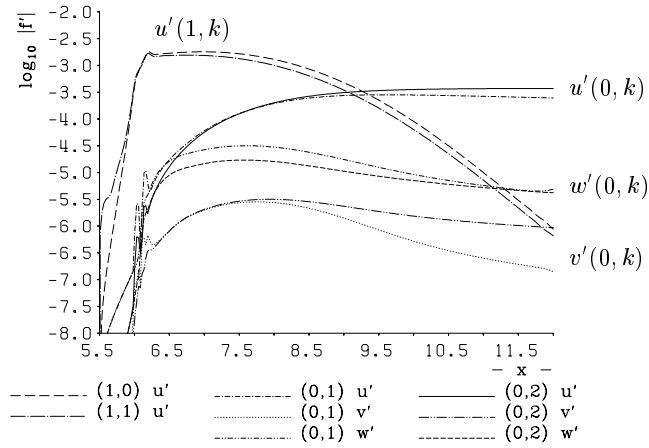


**Figure 2** Case 1: Downstream amplitude (max. over  $y$ ) development of the disturbance velocities; modes (1,0) and (1,1) disturbed at  $6.0 < x < 6.25$  at the wall; modes (0,1) and (0,2) nonlinearly generated.

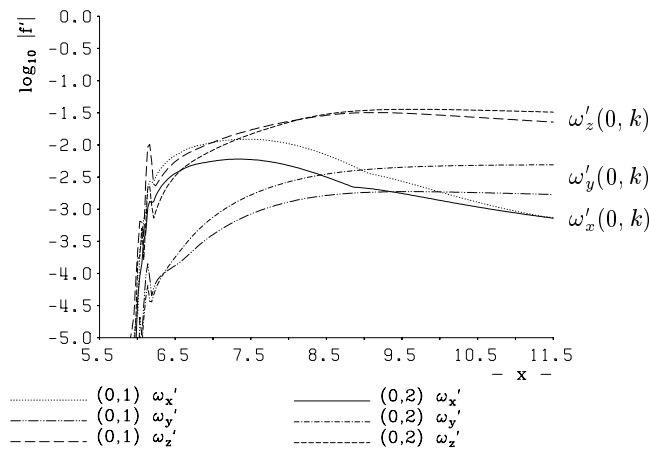


**Figure 3** Same as figure 2 but for disturbance vorticities.

The flow-field crosscuts (figs. 4 and 5) show that for both modes (0,1) and (0,2) swirling motions are present in the region of their generation, namely two counter-rotating longitudinal vortices per spanwise unit on top of each other close to the wall. This can be identified in figures a) by the coincidence of extrema of longitudinal vorticity  $\omega'_x$  with the center of swirling motions as indicated by the velocity vectors. Fluid is transported towards the wall from outside the boundary layer at e.g.  $z/\lambda_z = 0.25$  in fig. 5, is deflected at the wall and then flows away from the wall at  $z/\lambda_z = 0.0$  and  $z/\lambda_z = 0.5$ . Note that at the spanwise positions where fast fluid is brought towards the wall,  $u'$  is positive and where the normal velocity points away from the wall,  $u'$  is negative. Further downstream, where the modes have gone through a “relaxing” process without nonlinear forcing, the situation is different. Now only single swirling motions per spanwise unit are visible further from the wall in each case with the vortex center at  $y \approx \delta/2$ . If fig. 4b is compressed in the spanwise direction by a factor of 2, it looks much like fig. 5b. Hence, no principal differences between the modes (0,1) and (0,2) are present despite their different generation. The ratio of  $u'$  to the swirling motion, as indicated by  $v'$  and  $w'$ , is much larger for both disturbances at the position far downstream (note the disturbance-amplitude plots on the right of each figure).

The question rises whether a better characterization of the different steady 3-d deformation states exists. To this end, we employ the disturbance vorticity components (eq. 1):  $\omega'_x$  is a measure for longitudinal, and  $\omega'_y$  for wall-normal vorticity, where the latter is virtually  $\partial u'/\partial z$  since  $\partial w'/\partial x$  is relatively small. Thus, the ratio

$$\Omega = \frac{|\omega'_y|_{max}}{|\omega'_x|_{max}} \simeq \left| \left( -\frac{\partial u'}{\partial z} \right) \right|_{max} / \left| \left( -\frac{\partial w'}{\partial y} + \frac{\partial v'}{\partial z} \right) \right|_{max} \quad (3)$$

of the steady disturbance seems useful. It compares the strength of the  $u'$ -mode ( $\partial u'/\partial z$ ) with the longitudinal vorticity  $\omega'_x$  of the disturbance. For simplification, we have taken the maximum amplitude over  $y$ . Since for each spanwise mode  $f' \sim \hat{f}'_k \exp(ik\gamma z)$  and  $\partial f'/\partial z \sim k\gamma \hat{f}'_k$  ( $\hat{\cdot}$  - spectral amplitude) due to the spanwise periodicity, the right-hand side of eq. (3) simplifies to

$$rhs(3) = \frac{|\hat{u}'|_{max}}{\left| \frac{1}{k\gamma} \frac{\partial \hat{w}'}{\partial y} - \hat{v}' \right|_{max}}. \quad (4)$$

For  $k\gamma \gg 1$ ,  $\Omega \approx |\hat{u}'|_{max}/|\hat{v}'|_{max}$  could be conjectured, but this is never true, since  $|\hat{v}'|$  is always 3 to 4 orders of magnitude smaller than  $|\partial \hat{w}'/\partial y|$ . Hence

$$\Omega = \frac{|\omega'_y|_{max}}{|\omega'_x|_{max}} =: k\gamma K_s \simeq \frac{k\gamma |\hat{u}'|_{max}}{|\partial \hat{w}'/\partial y|_{max}} \quad (5)$$

defines a measure different from  $|\hat{u}'|/|\hat{v}'|$ .  $K_s$  effectively uses  $u'$  itself and not its spanwise gradient. In this paper we calculate  $\Omega$  and  $K_s$  directly from the respective maximal vorticity values. A further possible scaling with  $1/\delta$  is not used here.

Fig. 3 shows the streamwise amplitude (max. over  $y$ ) evolution of the vorticity components. Upon nonlinear generation,  $\omega'_x$ -modes are clearly enforced with  $\Omega \ll$

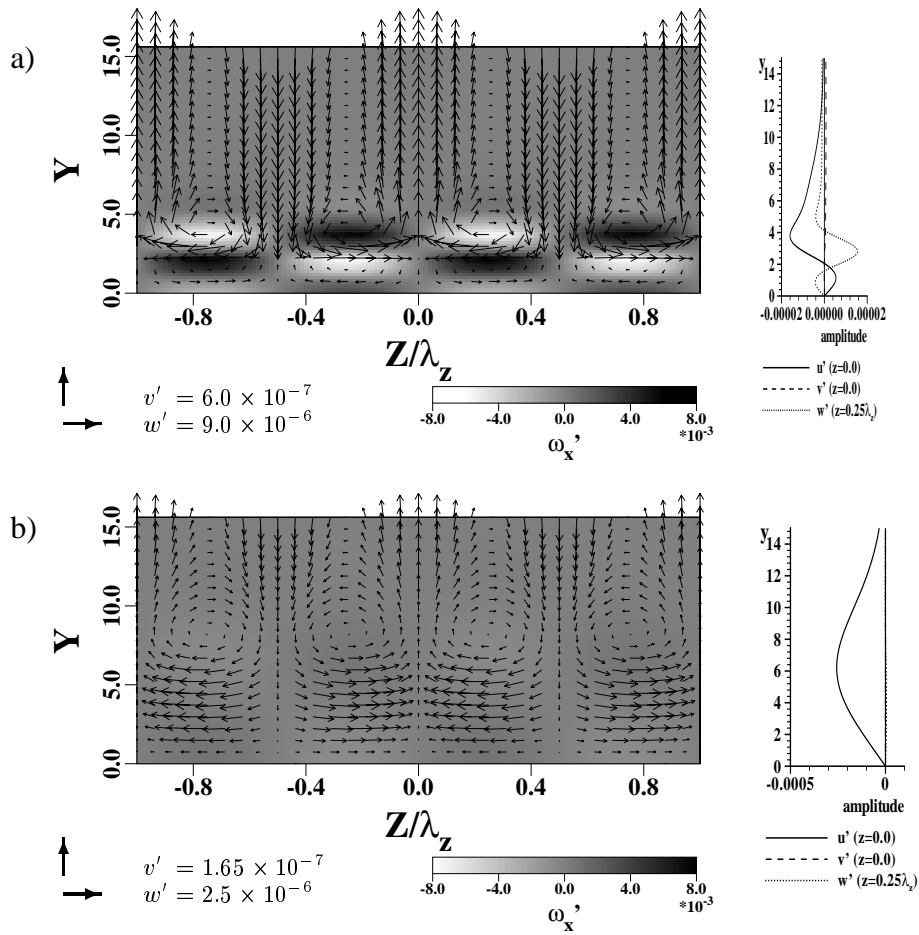


**Figure 4** Case 1: Wall-normal-spanwise distribution of  $v'$  and  $w'$  as vectors of mode (0,1) at a)  $x = 6.5$  and b)  $x = 11.5$ ;  $\omega'_x$  in grey scale.  $u'$ ,  $v'$  and  $w'$  as wall-normal velocity profiles to the right of the respective graphs. (The given values of  $y$  are stretched with  $\sqrt{Re}$ .)

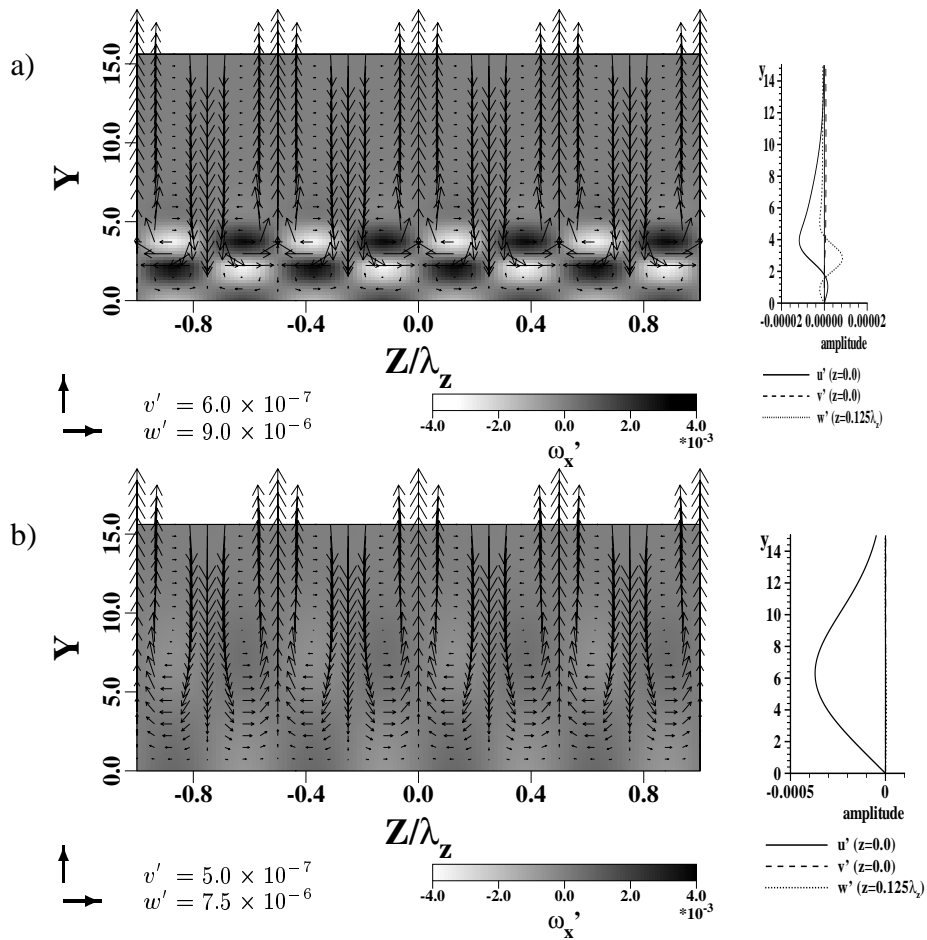


**Figure 5** Same as figure 4 but for mode (0,2).

1, and further downstream they relax into  $\omega'_y$ - or  $u'$ -modes with  $\Omega > 1$ . For (0,2),  $\omega'_y \geq \omega'_x$  downstream of  $x = 8.4$ , and for (0,1) downstream of  $x = 10$ . We find  $K_s$  which is  $\Omega$  normalized by  $k\gamma$  useful here because  $K_s \approx 0.003$  for both enforced  $\omega'_x$ -modes at  $x = 6.5$ , and  $K_s \approx 0.4$  for the  $u'$ -modes at  $x = 11.5$ . Thus we use  $K_s$  in the following, with the definition that  $u'$ -modes have a  $K_s$  value in the order of one.

### 3.2 Steady mode generated continuously upon nonlinearity: Oblique breakdown scenario

With the location of the disturbance strip slightly downstream of branch I ( $1.06 < x < 1.32$ ), case 2, the primary amplification of the (1,1) mode with low  $\gamma$  may be such that the continuous nonlinear generation of the (0,2) mode yields amplitudes higher than the amplitudes reached by eventual autonomous growth, and the ratio among the three disturbance velocity components is different (figure 6). The amplification rate  $\alpha_i$  of the mode (0,2) is twice the amplification rate of the generating mode (1,1), which is a strong indication for the enslaved existence of mode (0,2) by quadratic nonlinearity. Consequently, the (0,2)-amplitude increase during oblique breakdown does not represent the eventual autonomous growth of a  $u'$ -mode as found in case 1.

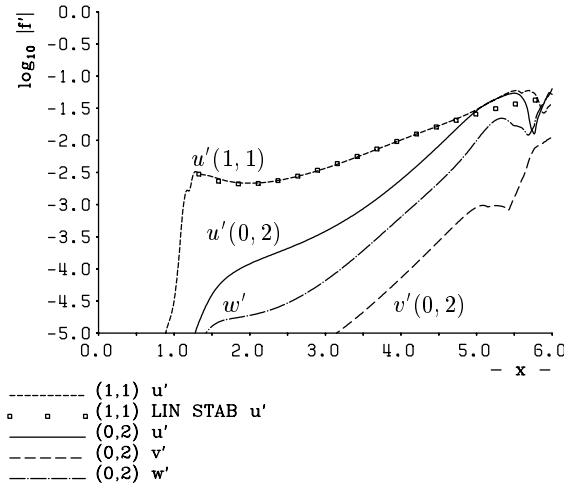


**Figure 6** Case 2: Downstream amplitude (max. over  $y$ ) development of disturbance velocities; mode  $(1, \pm 1)$  disturbed at  $1.06 < x < 1.32$  at the wall (oblique breakdown scenario).

Figure 7 reveals that up to  $x = 4.5$ ,  $K_s \approx 0.012$ , and within the following breakdown stage  $K_s$  decreases even to a value of 0.00015. Thus, (0,2) is a *longitudinal vortex mode* in this case, becoming strongly pronounced further downstream.

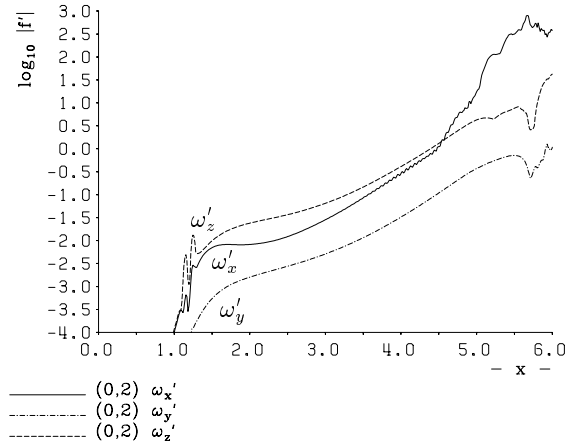


**Figure 7** Same as figure 6 but for disturbance vorticities.

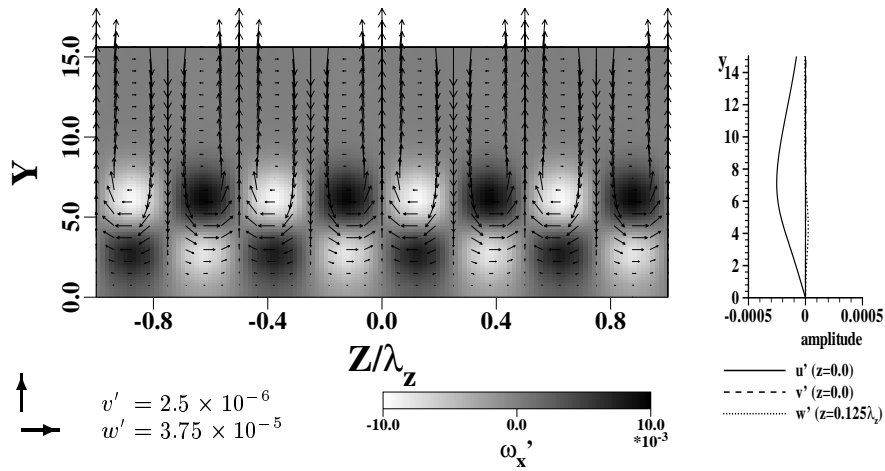


**Figure 8** Case 2: Wall-normal-spanwise distribution of  $v'$  and  $w'$  as vectors of mode (0,2) at  $x = 4.0$ ;  $\omega'_x$  in grey scale.  $u'$ ,  $v'$  and  $w'$  as wall-normal velocity profiles to the right of the respective graphs. (The given values of  $y$  are stretched with  $\sqrt{Re}$ .)

Nevertheless it is often termed “streak”-mode in discussions on the oblique breakdown scenario. For clarification recall the following: *i*) within oblique breakdown there exist lines  $z = \text{const.}$  where unsteady disturbance parts vanish since superposed and equal (1,1) and (1,-1) waves cancel the spanwise wave motion and form a standing wave in  $z$ -direction; thus “strips” in a flow visualization occur because they are only weakly blurred by unsteadiness; *ii*) as for flow physics, the present longitudinal vortex mode is clearly different from  $u'$ -Klebanoff-/“streak” modes. Both  $u'$ - and  $\omega'_x$ -modes can cause streaks in a flow visualisation: the latter by transporting streamwise momentum in wall-normal direction through the swirling motion, and the former by the relatively large  $u'$ -disturbance itself. The flow crosscut at  $x = 4.0$  (figure 8) is similar to fig 5 except for the distinct  $\omega'_x$ -extrema and the position of the swirl center ( $y \approx 3/4 \delta$ ). The difference is found in the relative strengths of the motions, expressed by  $\Omega$  or  $K_s$ .

### 3.3 Steady modes excited at the wall locally or continuously

The mode (0,2) can also be directly excited by the disturbance strip at the wall (figures 9 and 10). For local excitation, case 3, the  $u'$ -component of the disturbance now decays transiently up to  $x \approx 8.75$  and then grows very weakly; the ratios  $v'/u'$  and  $w'/u'$  are initially smaller but finally larger than in case 1. Fig. 10 reveals that local blowing/suction generates a  $\omega'_x$ -mode ( $K_s \simeq 0.015$  at the end of the strip) that rapidly relaxes into a  $u'$ -mode, with  $K_s \simeq 0.4$  for  $x > 9.5$ , cf. case 1.

In the case of continuous excitation ( $6 \leq x \leq 12.4$ ) with a straight line in the centre part of  $g_v(x)$  (see fig. 1), case 4,  $u'$  grows monotonously and is roughly one order of magnitude larger at the beginning than in case 3, but the weak growth is eventually identical. The respective  $\omega'$ -curves in fig. 10 make evident that continuous forcing with a spanwise pattern of alternating streamwise suction or blowing slits finally forces a pronounced  $u'$ -mode with growing  $K_s$  ( $K_s > 2.5$  for  $x > 11$ );  $K_s$  is larger than without persistent blowing/suction. Here it seems that the fixed  $v'$ -disturbance at the wall drives  $u'$  up, with a similar “relaxed” ratio  $|u'|/|v'| \simeq 150$  for both cases.

The flow-field crosscut of case 3 (fig. 11) shows the same qualitative picture as case 1. In case 4 (fig. 12) the disturbances at the wall can clearly be seen.

The influence of the spanwise wavenumber on the  $|u'|$ -growth is strong, and is shown in figure 13 for local excitation, cf. [7]. The growth is larger for smaller spanwise wavenumbers. For spanwise wavenumbers  $k\gamma > 13.2$  the respective modes decay in the considered domain. Note that  $\lambda_z \approx 2\delta - 3\delta$  is typically reported for the most amplified mode before branch I [7]. For the considered large  $Re_{\delta_1}$ , however,  $\delta(x=11.5)=0.045$ , and  $\lambda_z(0,2/3)=1.43$  ( $k\gamma=4.4$ ) and thus  $\lambda_z \approx 30\delta$  for largest amplification. The integral growth of this most amplified disturbance amounts to a factor of 13 between  $x = 7.5$  ( $Re_{\delta_1} = 1790$ ) and  $x = 22.5$  ( $Re_{\delta_1} = 3000$ ). The equivalent exponential growth rate ( $\alpha_i = -\frac{d}{dx} \ln A/A_0$ ) between  $x = 7.5$  and  $x = 15.0$  corresponds to about 1/5 the maximal Tollmien-Schlichting growth rate for Blasius flow. We note that the findings for  $k\gamma < 4.4$  have still to be confirmed.

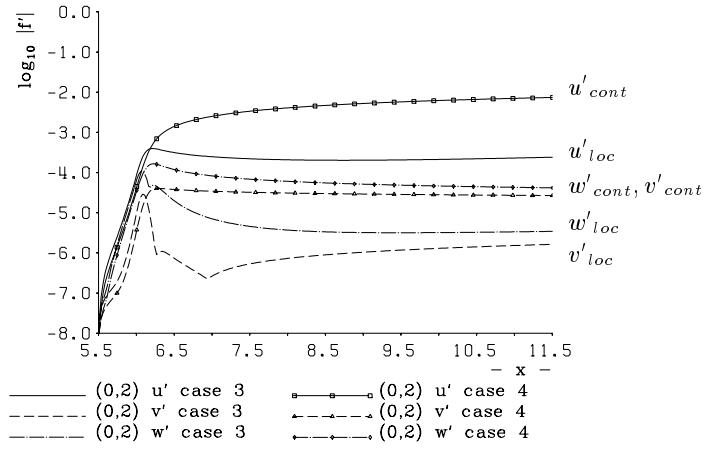


**Figure 9** Cases 3, 4: Downstream amplitude development of velocity components (max. over  $y$ ); case 3 (lines; mode (0,2) disturbed at  $6.0 < x < 6.25$  at the wall) and case 4 (lines with symbols; mode (0,2) continuously disturbed at the wall;  $6.0 < x < 12.4$ ) ( $k\gamma = 13.2$ ).

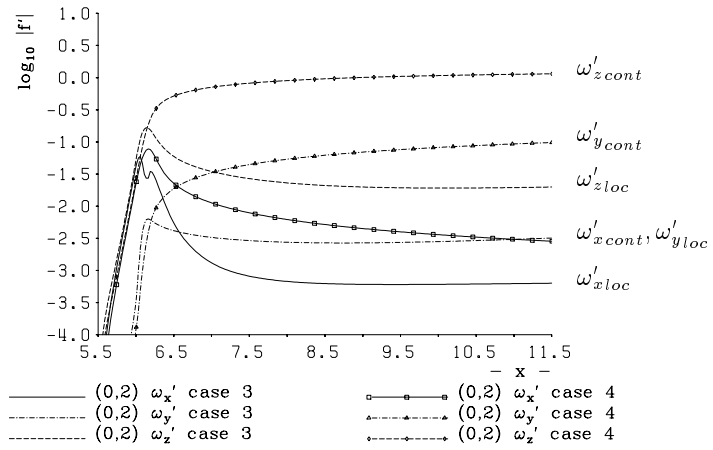


**Figure 10** Same as figure 9 but for disturbance vorticities.

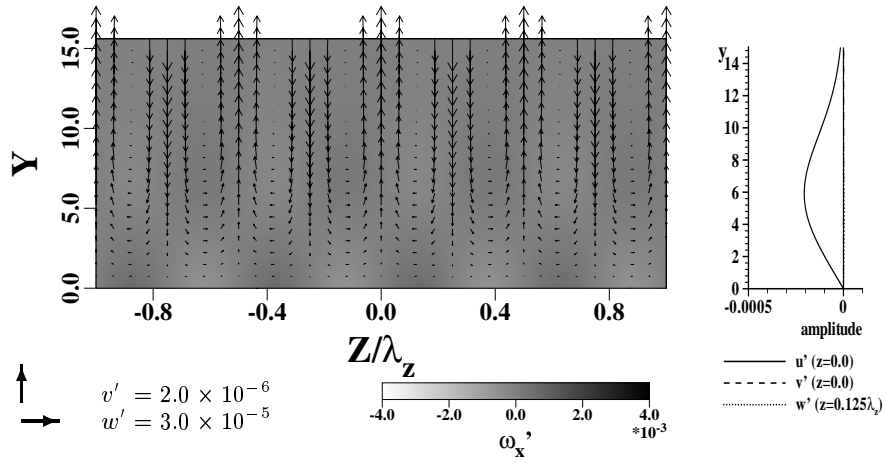


**Figure 11** Case 3: Wall-normal-spanwise distribution of  $v'$  and  $w'$  as vectors of mode (0,2) at  $x = 9.5$ ;  $\omega_x$  in grey scale.  $u'$ ,  $v'$  and  $w'$  as wall-normal velocity profiles to the right of the respective graphs. (The given values of  $y$  are stretched with  $\sqrt{Re}$ .)

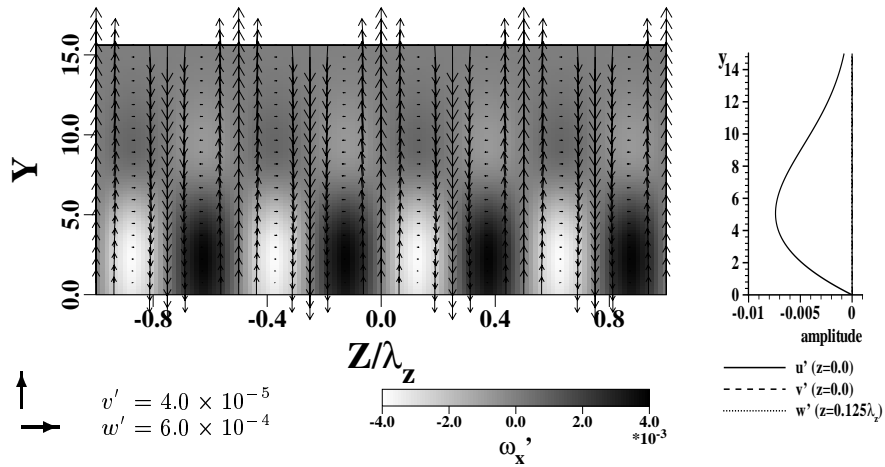


**Figure 12** Same as figure 11 but for case 4.

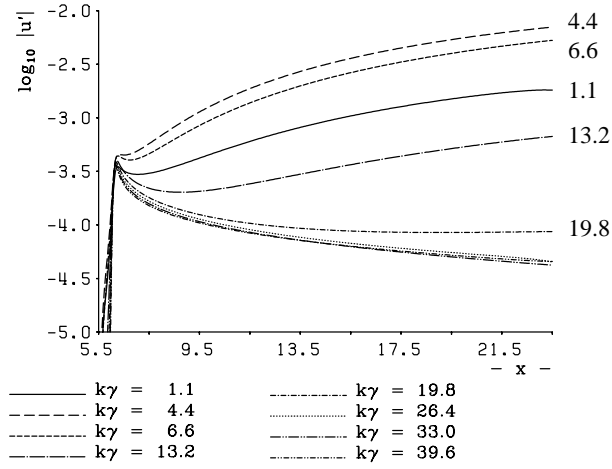


**Figure 13** Case 4: Downstream  $u'$ -amplitude (max. over  $y$ ) development; modes  $(0, k\gamma)$ ,  $1.1 < k\gamma < 39.6$  disturbed at  $6.0 < x < 6.25$  at the wall; note the extended length of the integration domain ( $x_N = 25.5$ );  $Re_{\delta_1}(x = 5.5) = 1552$ ,  $Re_{\delta_1}(x = 25.5) = 3343$ .

### 3.4 Steady modes in K-breakdown

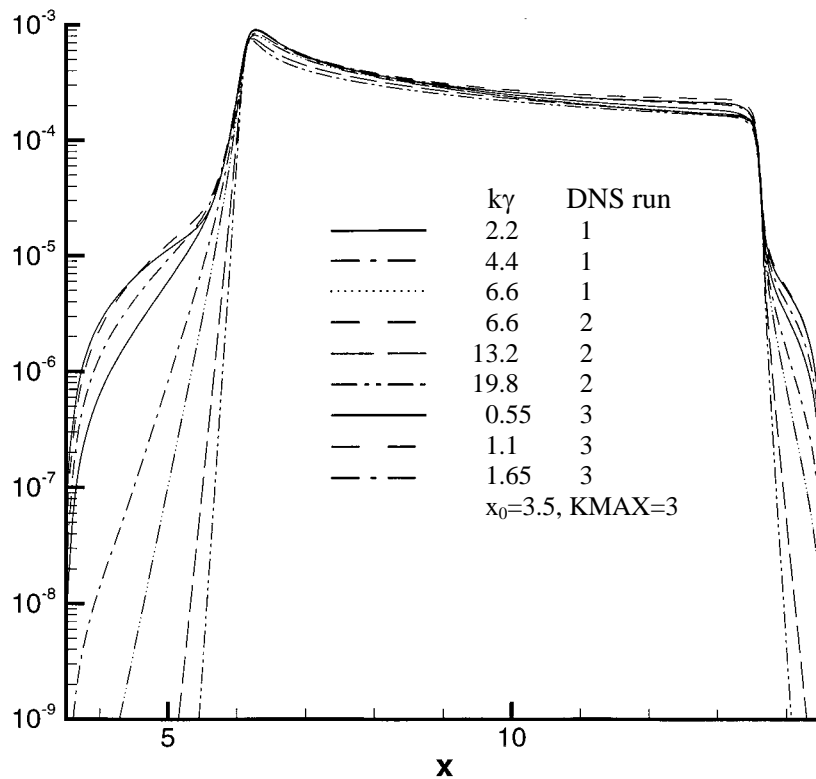
**Steady mode excited at the wall.** In a comparison to the previous results the K-breakdown scenario has been examined (fig. 14), where an unsteady 2-d wave  $(1,0)$  and a steady spanwise disturbance  $(0,1)$  are excited in the disturbance strip at the wall (case 5). First,  $u'(0, 1)$  transiently decays like in case 3, but downstream of  $x = 6.7$ , strong growth sets in. This is caused by the fundamental resonant interaction of  $(0,1)$  and the nonlinearly generated  $(1,1)$  with the priming mode  $(1,0)$  for  $u'(1, 0) \geq 2\%$ . A  $\omega'_x$ -mode with  $|u'| \approx 40 \cdot |v'| \approx 3 \cdot |w'|$  at  $x = 7.5$  develops. As known,  $(0,1)$  and  $(1,1)$  have about the same growth rate. In this scenario,  $(0,1)$  is a  $\omega'_x$ -mode by excitation and tries to relax in a  $u'$ -mode. It is eventually forced again to a  $\omega'_x$ -mode by the resonant mechanism.

**Steady mode generated continuously by nonlinearity.** An equivalent way to provoke the K-breakdown scenario has been investigated where the 2-d wave  $(1,0)$  and an unsteady 3-d wave  $(1,1)$  were excited within the disturbance strip at the wall (case 6, figs. 15 to 17).

The downstream development of the amplitudes of the unsteady disturbance mode  $(1,0)$  is almost indistinguishable from the one in case 6. The steady disturbance  $(0,1)$  is nonlinearly generated and gains in amplitude from the beginning up to the area of breakdown ( $x = 8.0$ ). Its character can be deduced from figure 16. From the very generation it is a  $\omega'_x$ -mode with  $K_s \approx 0.005$ ; only at transition,  $K_s$

Addendum to the results shown in Figure 13

- “Case 4” should read “Case 3 for various  $k\gamma$ ”.
- Careful simulations varying several numerical parameters of the base and disturbance flow revealed that the results shown for  $k\gamma < 26.4$  are influenced by the inflow position ( $x_0=5.5$ ) too close to the disturbance strip. The disturbance decay in upstream direction decreases with decreasing  $k\gamma$ , and interaction of the disturbances with the inflow boundary leads to modified wall-normal disturbance distributions above the disturbance strip for small values of  $k\gamma$ . The shown streamwise evolutions with growing amplitudes are *correct for the special disturbances generated locally above the disturbance strip in this case*, i.e. using any correct method for tracking their streamwise evolution will yield similar results. For  $x_0 < 4.0$  with unaltered disturbance-strip position, the influence of  $x_0$  vanishes, and the disturbance profiles above the strip do not depend any more on  $x_0$ . In this case all generated disturbances *decay* in downstream direction. Thus we find no growth for steady disturbances locally excited at the wall in the Blasius boundary layer at otherwise unforced conditions.



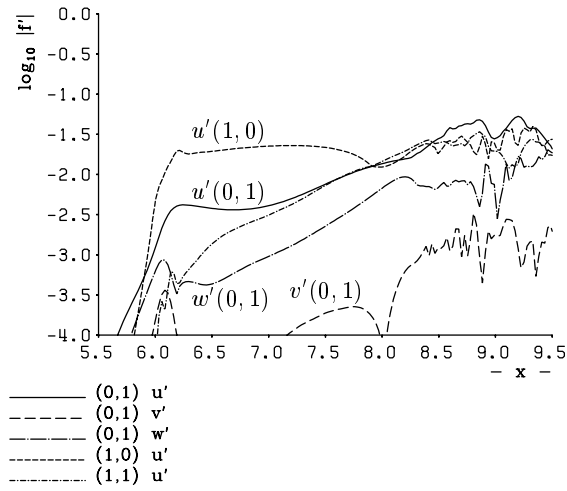


**Figure 14** Case 5: Downstream amplitude (max. over  $y$ ) development of disturbance velocities for K-breakdown initiated by modes (1,0) and (0,1), disturbed at  $6.0 < x < 6.25$  at the wall.

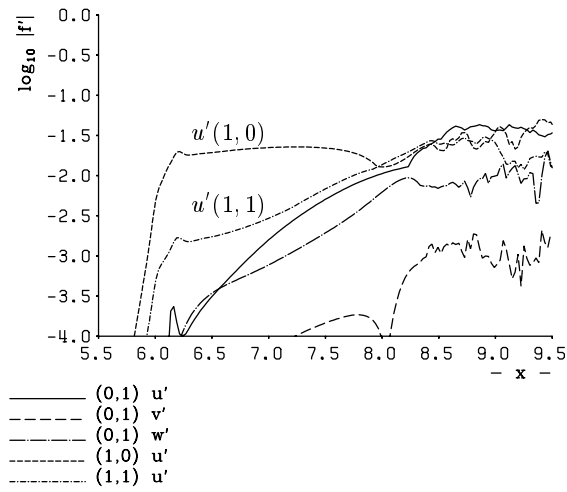


**Figure 15** Case 6: Downstream amplitude (max. over  $y$ ) development of disturbance velocities for K-breakdown initiated by modes (1,0) and (1,1), disturbed at  $6.0 < x < 6.25$  at the wall;  $\varphi(1,1) = 0$ .

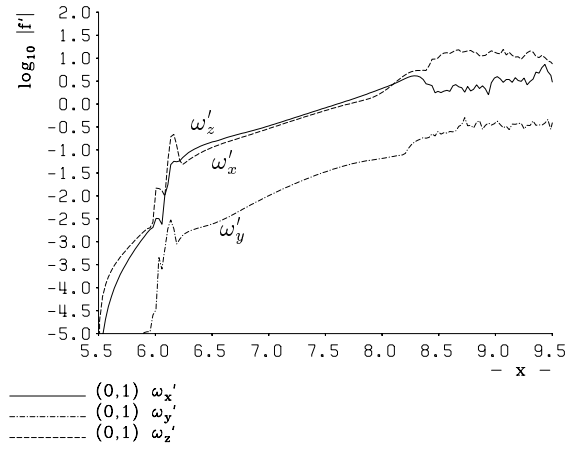


**Figure 16** Same as figure 15 but for disturbance vorticities.

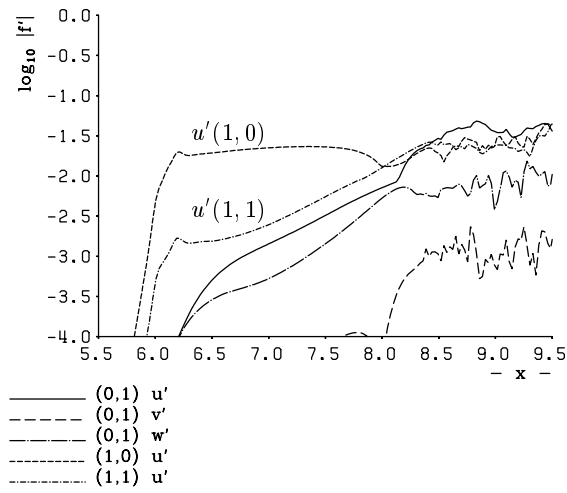


**Figure 17** Same as figure 15 but for  $\varphi(1,1) = \pi/2$ , case 7.

changes to a value of about 0.02. Unlike the oblique breakdown scenario,  $\omega'_x$  is surpassed here by  $\omega'_z$  finally. Moreover, “streaks” are more blurred due to the large unsteady 2-d fluctuation by the TS-wave (1,0).

In fig. 18, a crosscut (y-z plane) is shown at  $x = 6.4$ . Figure 18a) looks very much like fig. 4a); the two vortices on top of each other per spanwise unit obviously cause transient growth of  $u'(0, 1)$  in both cases. The longitudinal vortex mode visible in figure 18b) causes a swirling motion closer to the wall than (0,2) in the oblique scenario.

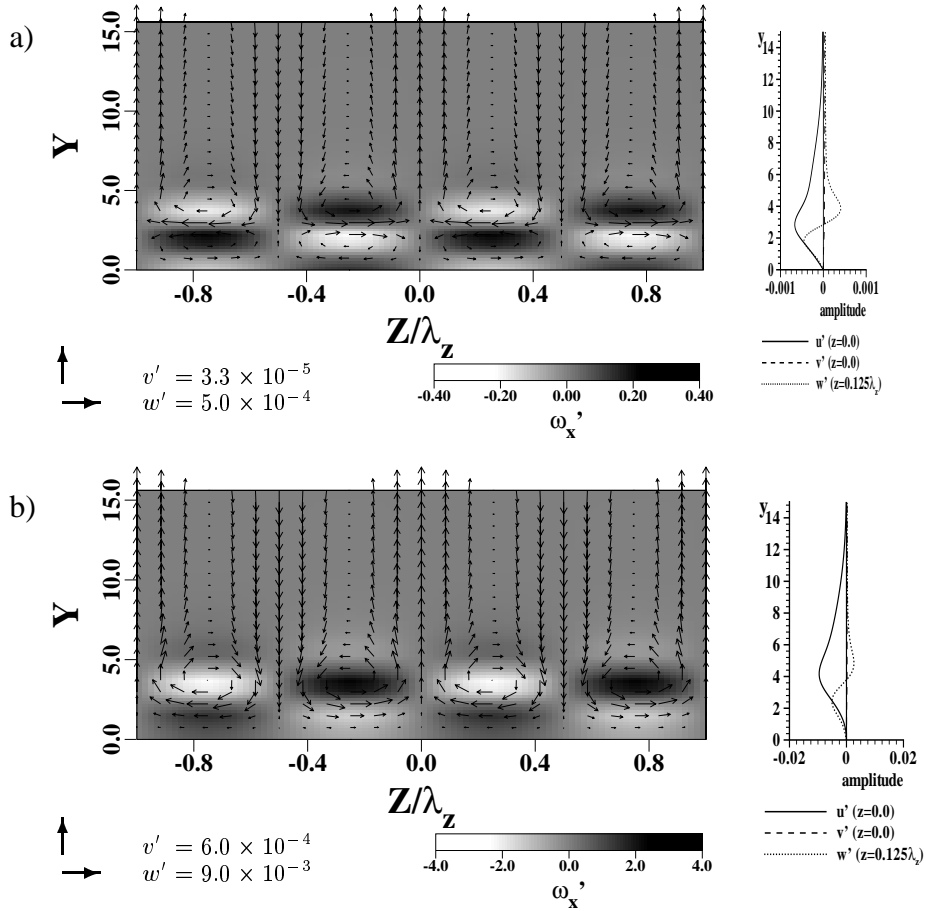


**Figure 18** Case 6: Wall-normal-spanwise distribution of  $v'$  and  $w'$  as vectors of mode (0,1) at a)  $x = 6.4$  b)  $x = 7.5$ ;  $\omega'_x$  in grey scale.  $u'$ ,  $v'$  and  $w'$  as wall-normal velocity profiles to the right of the respective graphs (boundary layer thickness  $\delta_{99.9\%}(x = 6.4) = 15.2$ ;  $\delta_{99.9\%}(x = 7.5) = 16.5$ ; the given values of  $y$  are stretched with  $\sqrt{Re}$ ).

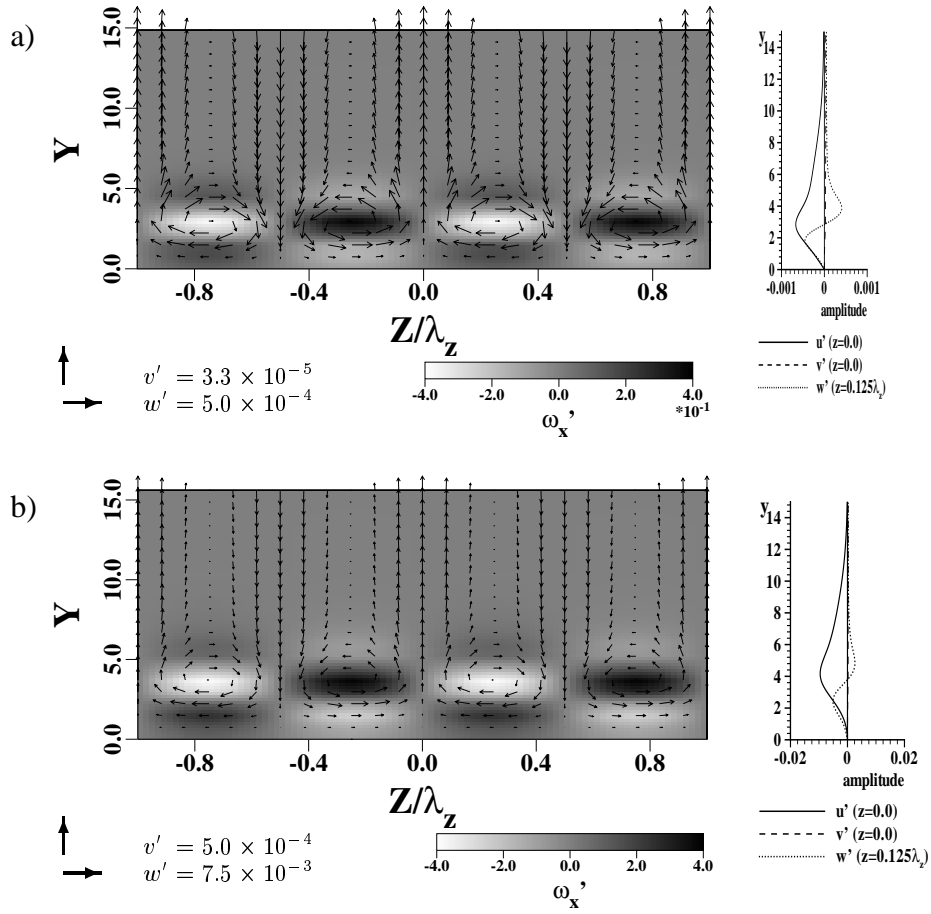


**Figure 19** Same as figure 18 but for case 7.

A notable influence parameter is the phase relation  $\varphi$  between the two excited modes (1,0) and (1,1) (see eq. 2). The amplitude development not only of the non-linearly generated mode (0,1) changes with different phase relation but also of the mode (1,1) (see figure 17, case 7). The modes (1,1) and (0,1) drop in amplitude by a factor of 1.6 (mode (1,1)) and by a factor of 2 (mode (0,1)) at  $x = 7.5$  with the identical excitation amplitudes as in case 6. The 2-d wave drops earlier in amplitude (downstream of  $x = 7.5$ ) compared to case 6. The ratio  $u'/v'/w'$  of the steady mode (0,1) is also different from the one in case 6. (We note that a phase relation of, e.g.,  $\varphi = \pi/3$  leads to amplitudes of (1,1) and (0,1) *larger* by a factor of 1.35 compared to case 6).

The double vortex system of fig. 18a is not present for the considered phase relation of  $\varphi = \pi/2$  (figure 19a). The steady mode (0,1) is generated in the same shape as it is present at resonant stages of transition at  $x = 7.5$  (figure 19b). Nevertheless, the amplitude level of the mode (0,1) is smaller than in the previous case.

## 4 Conclusions

1. **The first reaction** of the boundary layer to internal forcing of steady harmonic 3-d modes is a disturbance with dominant longitudinal vorticity, which we call  $\omega_x$ -mode. An  $\omega_x$ -mode is clearly characterized by a value of the ratio  $\Omega = |\omega'_y|_{max}/|\omega'_x|_{max}$  much smaller than 1, where  $\omega'_y$  is the wall-normal vorticity disturbance and a measure for the (spanwise gradient of the) streamwise velocity disturbance  $u'$ . This holds both for direct excitation at the wall by blowing/suction and for nonlinear generation through unsteady waves.
2. For **blowing/suction or local nonlinear forcing** the  $\omega'_x$ -mode rapidly relaxes to a  $\omega'_y$ - or  $u'$ -mode. A  $u'$ -mode is characterized by  $\Omega$  greater than 1, or more appropriately, the parameter  $K_s$  in the order of one, where  $K_s$  equals  $\Omega$  normalized by the spanwise wavenumber. Typically,  $|u'|_{max} \approx O(10^2 \sim 10^3)|v'|_{max}$ .
  - (a) Only by nonlinear generation of the steady disturbance this relaxation process is characterized by significant transient growth of  $u'$  where at the same time the wall-normal velocity disturbance  $v'$  grows much weaker or even decays. It seems that whenever the ratio  $|u'|/|v'|$  is smaller than some value, which we found to be of the order of 100, the  $u'$  amplitude is pushed up. In this sense  $v'$  is the driving force. This is in agreement with earlier investigations of other authors using theoretical approaches.
  - (b) However, the ratio  $|u'|/|v'|$  is not the only factor. In case of nonlinear generation in oblique breakdown or K-breakdown we find locally two swirling ( $\omega'_x$ ) motions on top of each other per spanwise unit close to the wall that cause significant transient growth of  $u'$ .
  - (c) Upon direct excitation at the wall no transient growth sets in since  $|u'|/|v'|$  is not too small and no double swirling motions are present.
  - (d) Rather, in case 2(c) long-range growth can set in, observed for  $Re_{\delta_1}$  larger than 1800, for a spanwise wavelength  $\lambda_z$  greater than 10 times the boundary-layer thickness  $\delta$ ; the maximal growth is for  $\lambda_z \approx 30\delta$ .
3. For **continuous nonlinear forcing** by growing unsteady waves, the  $\omega'_x$ -mode character of the steady disturbance is persistent. These modes can correctly be termed “longitudinal vortex modes”, as is done in some transition works. They represent counter-rotating vortical motions.
  - (a) At oblique breakdown the typical  $\omega'_x$ -mode “(0,2)” is characterized by  $K_s \approx 0.01$  in initial stages and the vortical motion is centered in the outer part of the boundary layer at about  $3/4 \delta$ .
  - (b) At K-breakdown, the typical  $\omega'_x$ -mode “(0,1)” is characterized by a slightly smaller  $K_s \approx 0.005$  and the vortical motion is centered at about  $1/4 \delta$ . For the persistent  $\omega'_x$ -mode in both 3(a) and 3(b)  $|u'| \approx 30|v'| \approx 3|w'|$ .

- (c) Streaks in flow visualisations are more likely to occur during oblique breakdown than during K-breakdown. In the oblique case they are not blurred by a large 2-d unsteady wave like during K-breakdown.
4. For both  $u'$ - and  $\omega'_x$ -modes the ratio of  $|v'|/|w'|$  is about 1/10, and thus flow-field crosscuts showing motions by  $v'$  and  $w'$  may look similar. The characteristic difference lies in the ratio of the streamwise vorticity to  $u'$  and can be expressed by the value of  $K_s$ .

If breakdown of a laminar flow is initiated by large-amplitude 3-d steady modes, the secondary instability (SI) mechanisms are *different* for  $u'$ -modes or  $\omega_x$ -modes. Despite the dominance of  $u'$  and its spanwise gradient in the SI mechanism, the other velocity components play also a role for both the shape and, to a large extent, the amplification rate of secondary instabilities. Recall that  $u'$ -modes can be triggered also by freestream turbulence, and longitudinal vortex modes by streamline or wall curvature, leading to crossflow vortices or Görtler vortices, respectively. As for secondary instability of crossflow vortices see, e.g., the article of Wassermann & Kloker in this book, and for a quantitative comparison of secondary instability theory and DNS the upcoming dissertation of G. Bonfigli, IAG.

The financial support of the Deutsche Forschungsgemeinschaft, DFG, under contract KI 890/4 is gratefully acknowledged.

## References

- [1] Andersson, P., Berggren, M., Henningson, D.S.: Optimal disturbances and bypass transition in boundary layers, layer, Phys. Fluids **11** 134 (1999).
- [2] Bakchinov, A.A., Grek, G.R., Klingman, B.G.B., Kozlov, V.V.: Transition experiments in a boundary layer with embedded streamwise vortices, Phys. Fluids **7**(4) 820 (1995).
- [3] Bertolotti, F.P.: Response of the Blasius boundary layer to free-stream vorticity, Phys. Fluids **9**(8), 2286 (1997).
- [4] Breuer, K.S., Kuraishi, T.: Transient growth in two- and three-dimensional boundary layers, Phys. Fluids **6**(6) 1983 (1994).
- [5] Criminale, W.O., Drazin, P.G.: The initial-value problem for a modeled boundary layer, Phys. Fluids **12**(2) 366 (2000).
- [6] Henningson, D.S., Lundbladh, A., Johansson, A.V.: A mechanism for bypass transition from localized disturbances in wall-bounded shear flows, J. Fluid Mech. **250**, 169 (1993).
- [7] Herbert, T., Lin, N.: Studies of boundary-layer receptivity with parabolized stability equations, AIAA-Paper 93-3053 (1993).
- [8] Kloker, M., Konzelmann, U., Fasel, H.: Outflow boundary conditions for spatial Navier-Stokes simulation of transition boundary layers, AIAA J. **31**(4), 620 (1993).
- [9] Luchini, P.: Reynolds-number independent instability of the boundary layer over a flat surface: Optimal perturbations. J. Fluid Mech. **404**, 289-309 (2000).
- [10] Stemmer, C., Kloker, M., Wagner, S.: Navier-Stokes simulation of harmonic point disturbances in an airfoil boundary layer, AIAA J. **38**(8), 1369 (2000).
- [11] Stemmer, C., Kloker, M.: Interference of wave trains with varying phase relations in a decelerated two-dimensional boundary layer, in Wagner, S., Rist, U., Heinemann, H.; Hilbig, R. (eds.): New Results in Numerical and Experimental Fluid Dynamics III. Vol. 77 of NNFM, Springer-Verlag, 239-246 (2002).